Key Engineering Materials
ISSN: 1662-9795, Vol. 969, pp 49-56
doi:10.4028/p-VbAbF9

Submitted: 2023-09-06
Accepted: 2023-09-19
Online: 2023-12-12

Model-Based Heat Input Control Validated on Martensitic Steel 1.4313

Indira Dey[1,2,a,*], Sergei Egorov[2,b], Fabian Soffel[1,c] and Konrad Wegener[2,d]

[1]Inspire AG, Technoparkstrasse 1, 8005 Zurich, Switzerland

[2]Institute for Machine Tools and Manufacturing (ETH Zürich), Leonhardstrasse 21, 8092 Zurich, Switzerland

[a]dey@iwf.mavt.ethz.ch, [b]egorov@iwf.mavt.ethz.ch, [c]soffel@inspire.ch, [d]wegener@iwf.mavt.ethz.ch

Keywords: Additive Manufacturing, Direct Metal Deposition, Martensitic steel, Heat Input Control

Abstract. The ability of direct metal deposition (DMD) to fabricate complex geometries is still limited. Especially in thin-walled structures heat accumulation can lead to intolerable geometric deviation and which has to be avoided. Combining thin walls and massive sections in one layer requires parameter adapting for each section within a layer. An existing semi-empirical model predicts the optimal process parameters for the austenitic steel 1.4404. This study demonstrates the validity of the model for martensitic steel 1.4313 by an experimental campaign. The demonstrators are characterized by a massive inner part attached to a thin-walled rib. They were fabricated by DMD using constant and adapted heat input and were qualified by visual inspection, geometrical accuracy, Vickers hardness, and microstructure analysis. The demonstrators built with the adapted laser power showed enhanced geometrical accuracy which is essential for post-processing. The hardness along the symmetry plane was significantly increased, especially in the thin wall section. The study confirms the applicability of the model for martensitic steel in terms of geometrical accuracy but identifies perspectives to integrate microstructural aspects into the model.

Introduction

Direct metal deposition (DMD) is a metal additive manufacturing (AM) technology where a laser creates a melt pool by melting the substrate and metal powder simultaneously. The created deposition is used to build parts. Compared to powder-bed processes, DMD has a higher buildup rate and the build space is only limited by the working chamber [1]. DMD aims to provide the ability to manufacture rapidly metallic, complex, and customized large structures [2]. However, its capabilities to build geometrically complex structures are still limited in terms of stability and geometrical accuracy. The underlying factors for a stable buildup are local heat transfer, powder catchment efficiency, surface shape, roughness, and oxide layers. Especially the combination of massive and thin-walled segments is endangering the process stability due to its individual powder catchment efficiency as reported by Eisenbarth et al. [3]. Therefore, adapted tool paths and process parameters are required to ensure part quality. Common approaches for parameter adaption are closed-loop control systems based on melt pool temperature measurements [4]. However, the control systems rely on sensors. Eisenbarth et al. [5] propose a semi-empirical model that does not rely on closed-loop control. They use experimentally gained data in combination with the actual part geometry. The algorithm creates a digital twin of the part from a given NC code, evaluates the massiveness of the section by calculating a local geometric factor, and alters the laser power accordingly. The model is fast and enables repeatable results avoiding trial and error experiments. They could validate the model with the austenitic steel 1.4404 and with various geometries. Until now, the transferability of his model was not validated for martensitic steel. However, martensitic steel is gaining more and more importance in turbo machinery parts due to its outstanding mechanical properties [6]. Furthermore, turbo machinery parts often have complex geometries with a differing cross section that serves the need for AM with martensitic steel parts. This study applies the model of Eisenbarth et al. [5] on a single wing demonstrator, with massive and thin segments, and martensitic steel 1.4313 in order to check the material transferability of the model. The results are evaluated in terms of geometrical accuracy, hardness, and microstructure.

Materials and Methods

Modeling Approach. The CAD model was created in Autodesk Fusion 360 with the technical drawing shown in Figure 1. For the DMD tool path calculation, a research CAM (RCAM) software developed by Eisenbarth et al. [7] was used. A contour feed rate of 250mm/min, a raster feed rate of 320mm/min, and a layer height of 0.8mm were used for both types of demonstrators based on a previously done 2D parameter study. The contour path is usually lower than the inner raster path to compensate for the worse catchment efficiency at the edge of a contour as described by Eisenbarth et al. [8]. Only the laser power was varied between 1000W and 490W for the demonstrator part with adapted laser power. The laser power for the demonstrator with constant laser power was set to 1000W as shown in Table 1.

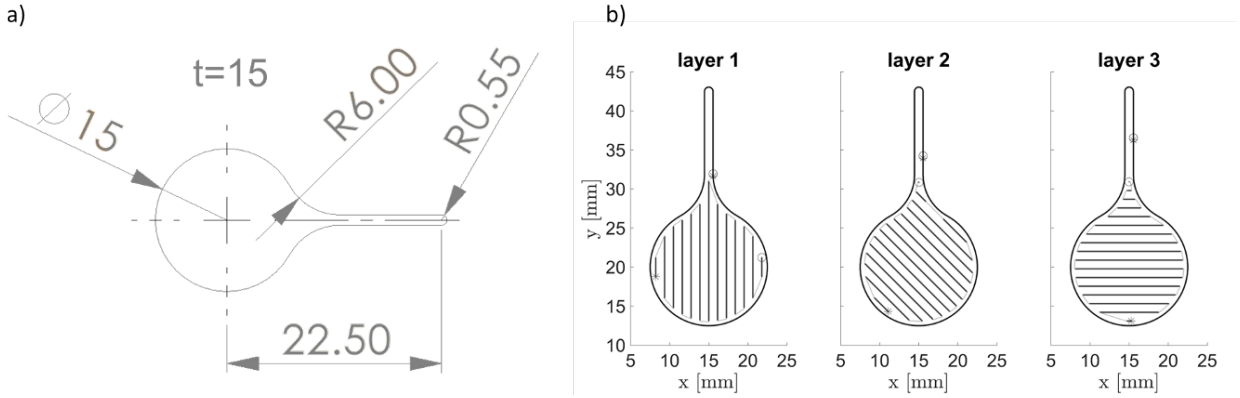

Fig. 1. (a) Geometry and (b) tool path of the single wing demonstrator.

Table 1. Process parameters for sample manufacturing.

No.	Powder mass flow	Feed [mm/min]	Laser Power	Process steps	Evaluation
1.1	P= 4g/min	Vc=250 Vr=320	Constant 1000W	DMD as built	Visual
1.2			Constant 1000W	DMD as built	2D laser scan
1.3			Constant 1000W	DMD as built	Cross section
2.1			Adapted	DMD as built	Visual
2.2			Adapted	DMD as built	2D laser scan
2.3			Adapted	DMD as built	Cross section

The RCAM software in MATLAB created the tool path for a given CAD model and added points at a constant distance, typically the size of the melt pool. For each point on the path, an adapted laser power based on the geometric factor κ is assigned to the NC code. κ is calculated by an algorithm which spans a control volume around the melt pool. The control volume has a circular shape in the lateral direction to eliminate directional dependence and a parabolic shape downwards. For each set point, the algorithm calculates the fraction of activated elements inside the control volume further described in [5, 7]. Thus, κ is a measure for the massiveness of the surrounding. κ=1, if the control volume is completely filled by surrounding material. Exemplary, at the top edge of the thin wall in the single wing geometry, κ reaches a minimum of 0.17. The lower the geometric factor κ, the lower the applied laser power. In the first layers, the laser power is the highest. K is correlated to the laser power, with 1000W for $\kappa = 1$ and 490W for $\kappa = 0$, assuming that the overall workpiece temperature remains constant.The geometric factor and the resulting laser power adaption of the model are shown in Figure 2.

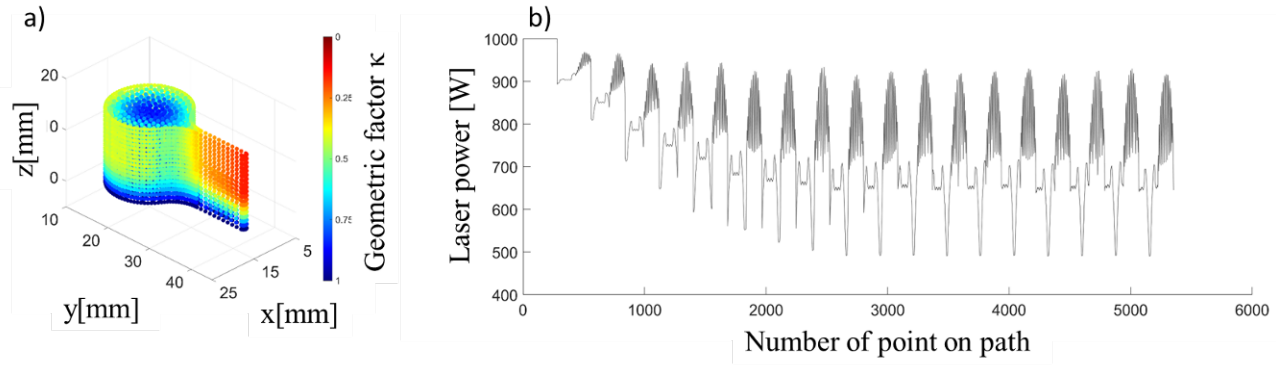

Fig. 2. Laser profile of the digital twin.

Experimental Validation

Machine Settings. The experiments were carried out on a 5-axis machining center Mikron HPM450U by GF Machining Solutions. The machining center was equipped with an IPG Photonics 1 kW YLR-1000 fiber laser system and a Hybrid Manufacturing Technologies (HMT) processing head that can deposit welding tracks with a width of approximately 2.2mm. Mild steel S235JRC (1.0122) plates were used as substrate and gas-atomized 1.4313 powder from Oerlikon Metco as deposit material. Argon was used as a powder carrier gas with a volume flow of 4l/min and shielding gas with a volume flow of 8l/min during the deposition process.

Geometrical Accuracy. The height profiles along the symmetry plane of the DMD specimens were measured with the laser line sensor scanCONTROL 2900-50/BL from Micro-Epsilon.

Microstructure Analysis. The specimens were cut on their vertical symmetry plane, hot-mounted, and polished on a ATM Saphir 520 machine. Polishing cloths and polycrystalline diamond suspension down to a grain size of 3 µm were used with a constant force of 10 N and a speed of 200 rpm. The specimens were then cleaned in an ultrasonic ethanol bath, and etched by immersion in Kalling II. Cross-sectional images were taken with a light microscope Keyence VHX-5000. The light microscopy was taken with two different lightning settings. With the dark field lightning, the grains are visible, and with the bright field the pores are visible.

Hardness Measurement. Vickers hardness was measured on an ATM Qness Q10 M device, with a load of 100 g and a dwell time of 15 s. The indentations were aligned according to Figure 3 resulting in 15 points with a distance of 5mm from each other along the symmetry plane.

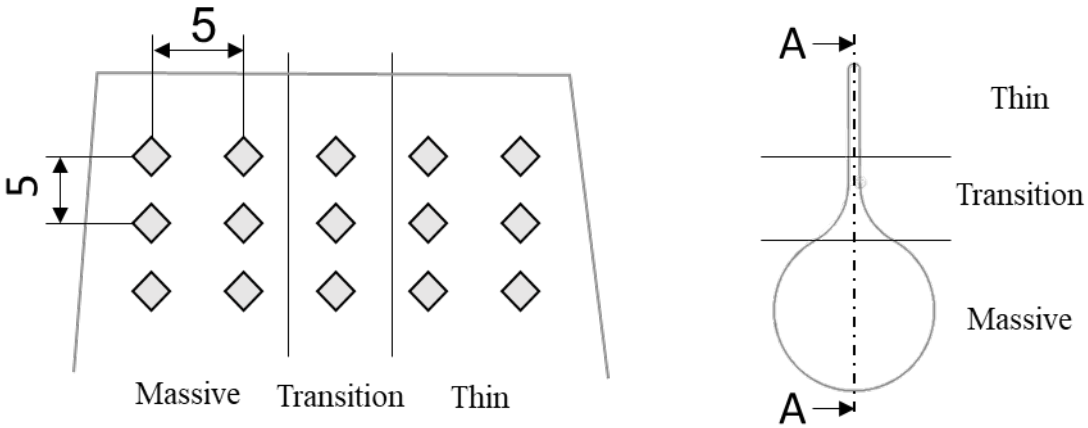

Fig. 3. Hardness measurement point.

Material. The martensitic stainless steel EN X3CrNiMo13-4 (1.4313) was used as powder material. The chemical composition is described in Table 2.

Table 2. Chemical composition of 1.4313 [wt%] referring to Oerlikon Metco.

Cr	Ni	Mn	Mo	Si	N	O	C	S	P	Fe
13.07	4.01	0.53	0.49	0.31	0.03	0.028	0.02	0.003	0.003	Bal

Results and Discussion

Experimental Validation.

Geometrical Accuracy. It is visible by eye that the specimens with an adapted laser power resulted in a more even top surface compared to the specimens built with the constant laser power as shown in Figure 4 a). The reason is that with constant laser power, especially the thin-walled section, heated up, the melt pool size increased, the liquid material run off the side due to the force of gravity and resulted in a bulky surface during solidification as shown in Figure 4 c). The overheating led to an increase in the width of the thin-walled section and a larger layer edge curvature of the massive section as shown in Figure 4 d).

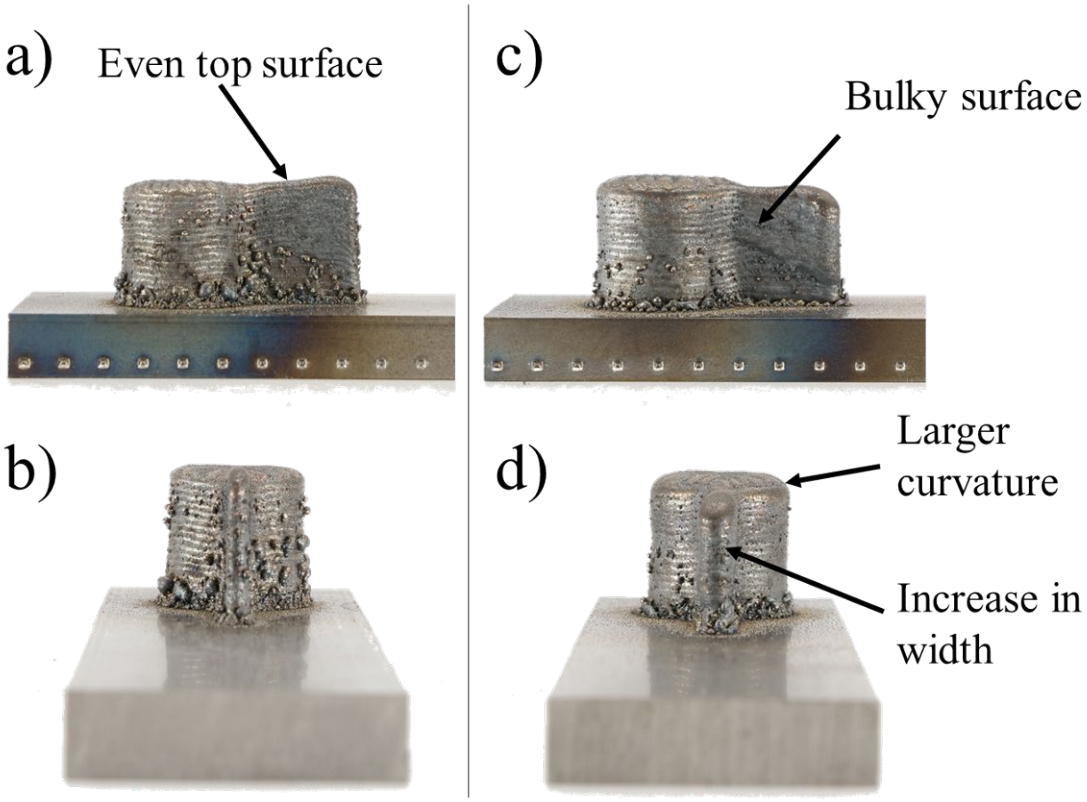

Fig. 4. Visual inspection of the single wing demonstrator a) side view and b) front view with adapted laser power c) side view and d) front view with constant laser power.

2D Laser Scan. The 2D scans confirmed in **Figure 5** that the thin-walled section of the specimen with constant laser power did not meet the nominal height of 15mm and therefore cannot be post-processed by subtractive milling anymore. Hence, if subtractive post-processing is required, it is beneficial to aim for an overbuild rather than an underbuild. The maximal deviation of the height d_a from the overall height 15mm with adapted laser power was 2mm compared to d_c of 3.9mm with constant laser power.

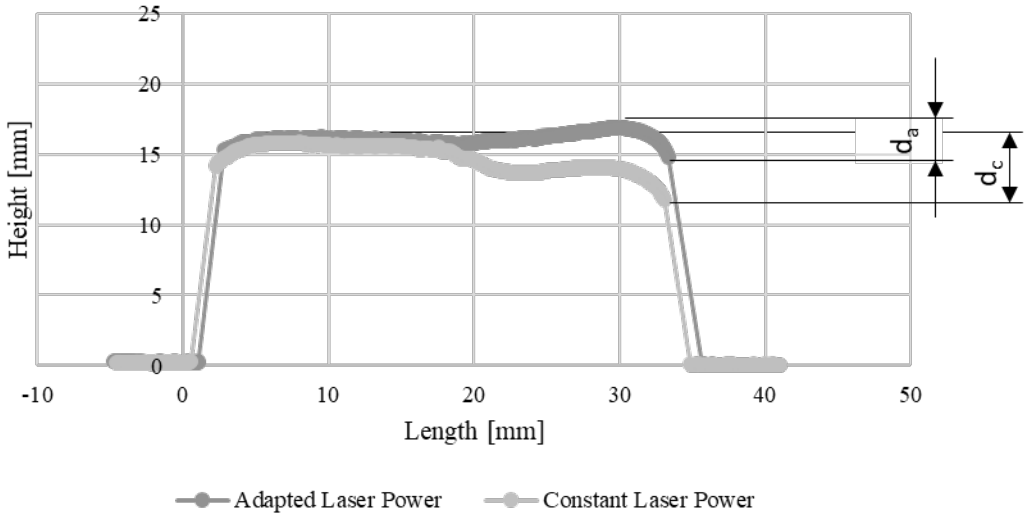

Fig. 5. 2D laser scans along the symmetry plane.

Microstructure Analysis. The specimen made with adapted laser power display a homogeneous microstructure as shown in Figure 6 a), consisting of fine martensitic laths. This can be commonly explained by lower temperature gradients that result in finer grains along the local temperature gradient [9].

The specimen with constant laser power displays two different solidification structures depending on the section as shown in Figure 6 c). The bulk section is made of fine grains, while elongated and coarser grains across several layers in the buildup direction are observed in the thin wall section. This can be explained, according to Khodabakhsh et al. [10], by the increase of peak temperatures and reduced cooling rates due to the lower conductivity in the thin walled section. A large temperature gradient and successive remelting of the previous layer leads to an elongated grain growth in the building direction. The reduced cooling rates in the thin walled section were observed by a thermal camera in both of the specimens.

Furthermore, porosity along a vertical line in the transition zone could be observed in the specimens made with adapted laser power as shown in Figure 6 b). Since the pores are non-spherical indicating a lack of fusion and only appear the transition zone, it can be assumed that the hatch distance of the tool path between the massive and thin-walled section is not sufficient. Changing to a continuous tool path pattern or higher laser power could reduce the porosity.

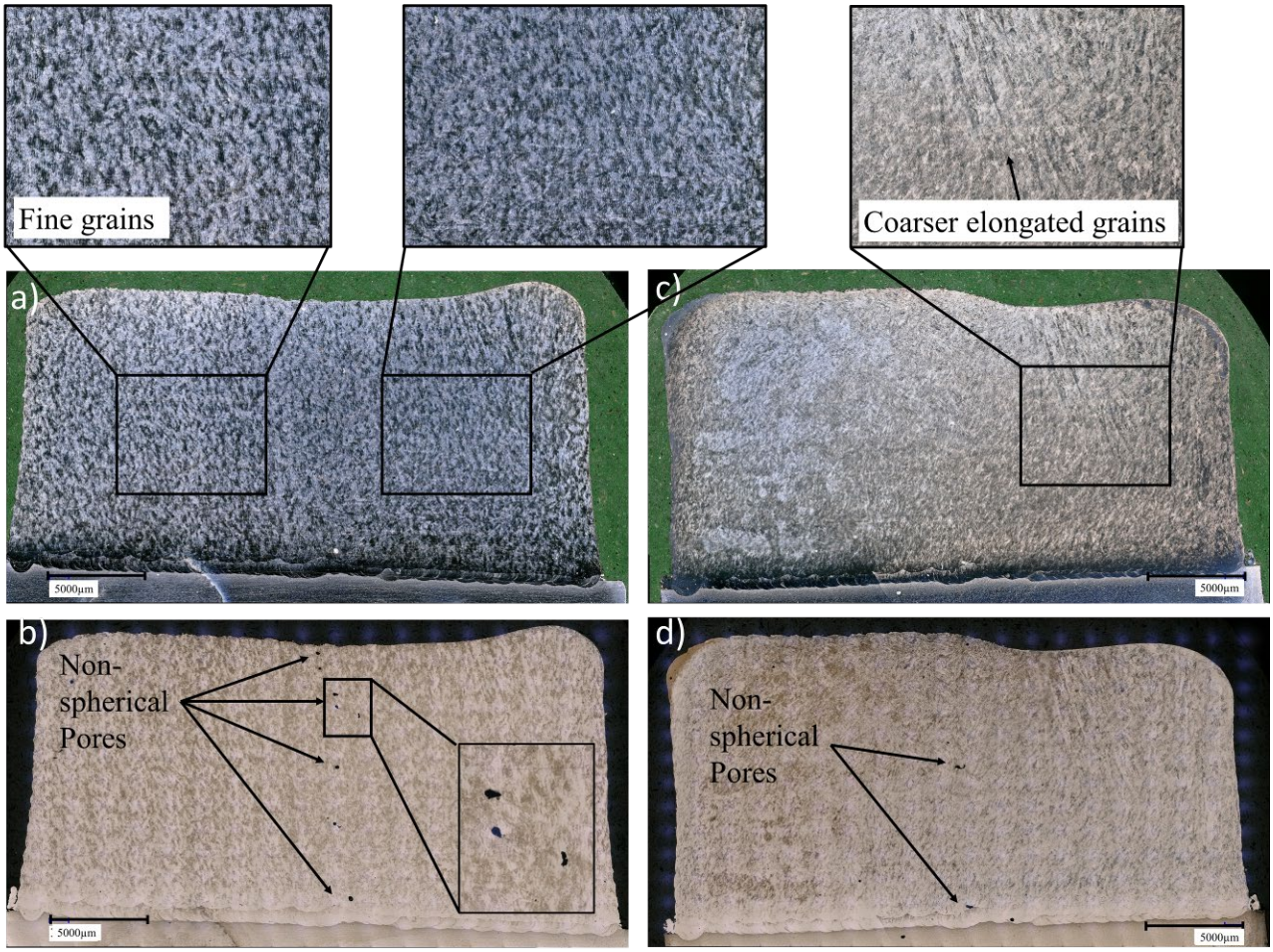

Fig. 6. Microstructure of the single wing demonstrator a) dark field b) bright field lightning and adapted laser power, c) dark field d) bright field lightning and constant laser power.

Hardness Measurement. The hardness measurements of the specimens with adapted laser power, displayed in Figure 7, showed that the hardness increased from the massive section up to the thin-walled section. The diagonals of the imprint had a size around 20 µm. According to the Hall-Petch rule [11], a homogenous microstructure indicates homogenous mechanical properties and a finer microstructure would lead to higher hardness. However, a grain refinement could not be deteced by light microscopy sufficiently. Electron Backscatter Diffraction (EBSD) grain mapping is necessary to reliable measure the grain size. Another explanation, according to Colaco and Vilar [12], is that a lower heat input increases austenite formation in soft-martensitic steel. Niederau [13] claims that the austenitic range extends at 12-15% chromium and 4-5% nickel to about 600°C. Layerwise reheating of the part leads to a comparable temperature as annealing. Annealing around 600°C can lead to fine dispersive austenite which is not visible in light microscopy but results in very good ductility. However, no statement about the martensite fraction which mainly influences the hardness was made.

Furthermore, the hardness of the specimens with the constant laser power did not change significantly between the massive and thin-walled sections although the microstructure showed larger grains within the thin-walled section. This leads to the assumption that the Hall-Patch rule cannot be easily applied to martensitic welded structures as discussed by Lehto et al. [14]. In summary. the hardness increased with a lower heat input and stayed constant with a constant heat input in the thin-walled section. This leads to the assumption that the martensite formation that mainly affects the hardness is mostly driven by the local heat flow during the solidification of the a melt pool and less by the global heat flow and geometry. Future research should conduct global/local temperature measurement and X-ray diffraction (XRD) to indicate retained austenite.

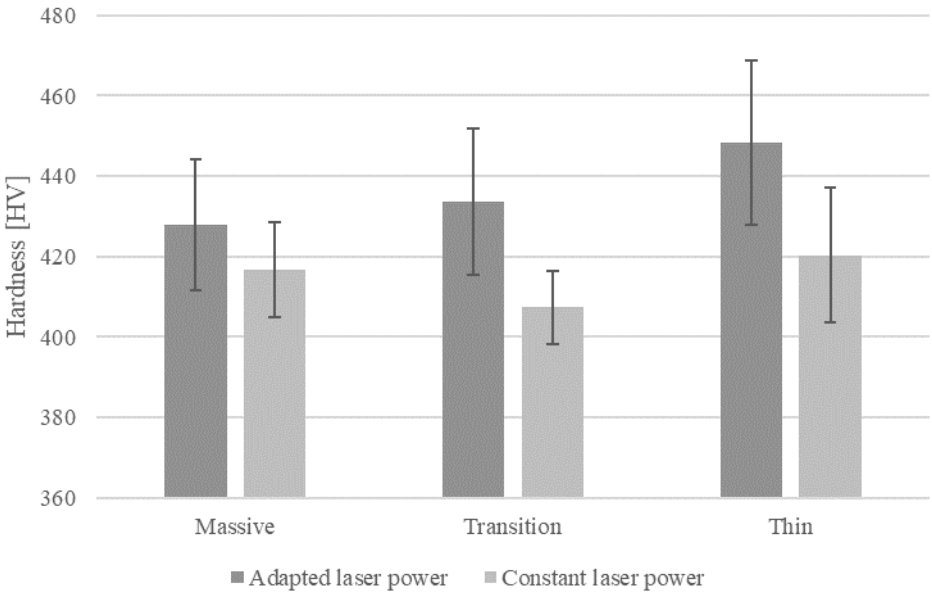

Fig. 7. Vickers hardness measurement of the specimens.

Conclusion

The study successfully validated the semi-empirical model of Eisenbarth et al. [5] on a single wing demonstrator part made of martensitic steel 1.4313. The resulting laser power adaption led to an improvement in geometrical accuracy, which could be confirmed with the height measurements of a 2D laser scanner. The laser power adaption achieved the nominal height and improved geometrical accuracy, which is essential for post-processing. With a lower heat input, a homogenous microstructure could be achieved in which the hardness increased. With a constant heat input, a heterogenous microstructure with elongated grains could be achieved in which the hardness remained constant. This led to the assumption that the Hall-Patch rule cannot be easily applied to deposited martensitic steel and the martensitic transformation is mainly affected by the local heat flow within a melt pool instead of the global heat flow of the part. Furthermore, non-spherical pores were visible in the transition zone which was possibly caused by an inadequate tool path planning. The study showed that the model could be used to adapt the laser power to primarily achieve geometrical accuracy. Nevertheless, the microstructural outcome is not considered in the heat input model. For future research, XRD and EBSD mapping are suggested to answer the questions about the grain size and phase changes. Moreover, the temperature history and cooling rates during manufacturing could be changed by altering the model in terms of control volume, geometrical factor and laser power, to modify the hardness of the material.

References

[1] A. Dass and A. Moridi: in *Coatings,* vol. 9, no. 7, 2019

[2] T. DebRoy *et al.*: in *Progress in Materials Science,* vol. 92, pp. 112-224, 2018

[3] D. Eisenbarth, F. Soffel, and K. Wegener: presented at Lasers in Manufacturing, Munich, Germany, 2019

[4] Z. Smoqi *et al.*: in *Materials & Design,* vol. 215, p. 110508, 2022

[5] D. Eisenbarth, F. Soffel, and K. Wegener: presented at the Additive Manufacturing in Products and Applications (AMPA), Zurich, Switzerland, 2019

[6] F. Badkoobeh, H. Mostaan, M. Rafiei, H. R. Bakhsheshi-Rad, and F. Berto: in *Metals,* vol. 12, no. 1, p. 101, 2022

[7] D. Eisenbarth: Doctoral Thesis, Institut für Werkzeugmaschinen und Fertigung, ETH Zürich, Zürich, 2020.

[8] D. Eisenbarth, P. M. Borges Esteves, F. Wirth, and K. Wegener: in *Surface and Coatings Technology,* vol. 362, pp. 397-408, 2019

[9] A. Leicht: Doctoral Thesis, Chalmers Tekniska Hogskola, Sweden, 2020.

[10] F. Khodabakhshi, M. H. Farshidianfar, A. P. Gerlich, M. Nosko, V. Trembošová, and A. Khajepour: in *Additive Manufacturing,* vol. 31, p. 100915, 2020

[11] E.O. Hall: in *Proc. Phys. Soc. Ser. B*, 1951, vol. 64, pp. 747-753.

[12] R. Colaço and R. Vilar: in *Materials Science and Engineering: A,* vol. 385, no. 1-2, pp. 123-127, 2004

[13] H. Niederau: in *Stahl u. Eisen*, vol. 98, 1978, pp. 385-392.

[14] P. Lehto, H. Remes, T. Saukkonen, H. Hänninen, and J. Romanoff: in *Materials Science and Engineering: A,* vol. 592, pp. 28-39, 2014

The publication of this article was funded by the ETH Zurich 10.13039/501100003006